Resonant Auger decay studies in Kr $3d^{-1}_{3/2,5/2}np$ states using angle-resolved electron imaging spectroscopy

A. Farhat,[1] A. A. Wills,[1] B. Langer,[2,*] and N. Berrah[1]
[1]*Physics Department, Western Michigan University, Kalamazoo, Michigan 49008*
[2]*Fritz-Haber-Institut der Max-Planck-Gesellschaft, Faradayweg 4-6, D-14195 Berlin, Germany*
(Received 23 June 1998)

An extensive and detailed mapping of the resonant Auger decay of all the photoexcited $3d^{-1}_{3/2,5/2}np$ states in Kr has been performed using angle-resolved two-dimensional photoelectron spectroscopy at the Advanced Light Source at Lawrence Berkeley National Laboratory. This has allowed us to obtain angular distributions and spectator and shake probabilities for the Kr $3d^{-1}np \rightarrow 4s^{-1}4p^{-1}(^1P)mp+e^-$ ($n=5-9$, $m=5-11$) resonance Auger decays. The results show that the spectator-core coupling is strong at lower n ($n=5,6$) but lessens for higher n, with a shake-up of $m=n+1$ preferred. The observed trend is in good agreement with the previous experimental and theoretical spectator and shake probabilities for these transitions and also with the analogous decay to the $4s^24p^4mp$ states [H. Aksela *et al.*, Phys. Rev. Lett. **25**, 4970 (1997)]. However, to our knowledge, no prior angular distribution measurements for the Kr $3d^{-1}np \rightarrow 4s^{-1}4p^{-1}(^1P)mp+e^-$ ($n=5-9$, $m=5-11$) resonant Auger decay has been reported. These are found to also show similar behavior to the decay to the $4s^24p^4mp$ states. [S1050-2947(99)02301-X]

PACS number(s): 32.80.Dz, 32.80.Fb, 32.80.Hd

I. INTRODUCTION

When a core electron is excited into an unoccupied orbital, the resulting excited states decay via Auger-like transitions. These can be summarized, in the case of the $3d \rightarrow np$ transitions in Kr, into five main groups as follows:

(a) $3d^9np \rightarrow 4s^24p^5+e^-$
(b) $3d^9np \rightarrow 4s^14p^6+e^-$
} participator Auger decay

(c) $3d^9np \rightarrow 4s^24p^4n'l+e^-$
(d) $3d^9np \rightarrow 4s^14p^5n'l+e^-$
(e) $3d^9np \rightarrow 4s^04p^6n'l+e^-$
} spectator Auger decay $\begin{cases} n'<n & \text{shake-down} \\ n'=n & \text{strict spectator} \\ n'>n & \text{shake-up.} \end{cases}$

The Auger decay spectra of krypton at the $3d \rightarrow 5p$ resonance and of xenon at the $4d \rightarrow 6p$ resonance were reported by Eberhardt, Kalkoffen, and Kunz [1]. Since then, the resonant Auger spectra of rare gases have been a subject of intense investigation both experimentally and theoretically [2–10]. The achievable photon energy and electron resolutions have made it difficult to perform detailed quantitative measurements that are differential in energy and angle. However, recent improvements have enabled some studies to distinguish unambiguously many of the populated final states [6,7,11,12] and their angular distributions in the case of the Xe $4d_{5/2} \rightarrow 6p$ [11] and Ar $2p \rightarrow ns,d$ [12] resonances.

The Auger decay of resonantly excited states in the rare gases is usually dominated by the spectator type where the inner-shell electron is excited to one of the Rydberg orbitals described by the corresponding quantum numbers n,l,j [(c)–(e)]. The electronic core relaxes by an Auger transition that exposes the Rydberg electron to a different field from the ionic core as it changes from singly to doubly charged. As a result, it may change its quantum numbers $n \rightarrow n'$, $l \rightarrow l'$, and $j \rightarrow j'$. If $n=n'$, we would have a pure spectator transition, but if $n<n'$, we would have a shake-up transition and if $n>n'$, we would have a shake-down transition. The Rydberg electron may also participate in filling the core hole, which leads to the single-hole final ionic states, in which case we would have participator transitions (a) and (b). It has been shown that the spectator transitions are overwhelmingly stronger than the participator transitions [13]. Åberg [14] formulated the shake model to explain successfully the shake contributions in the resonant Auger spectra. He introduced a complete theoretical treatment for the shake theory, including electron correlation in both the ground and final states. Martin and Shirley [15] demonstrated the importance of including correlated many-electron wave functions for both the initial and final states where the final-state wave functions must be orthogonal to each other. This theory was later for-

*Present address: Techniche Universität Berlin, Institut für Atomar und Analytische Physik, Sekretariat PN 3-2 Hardenbergstrasse 36, 10623 Berlin, Germany.

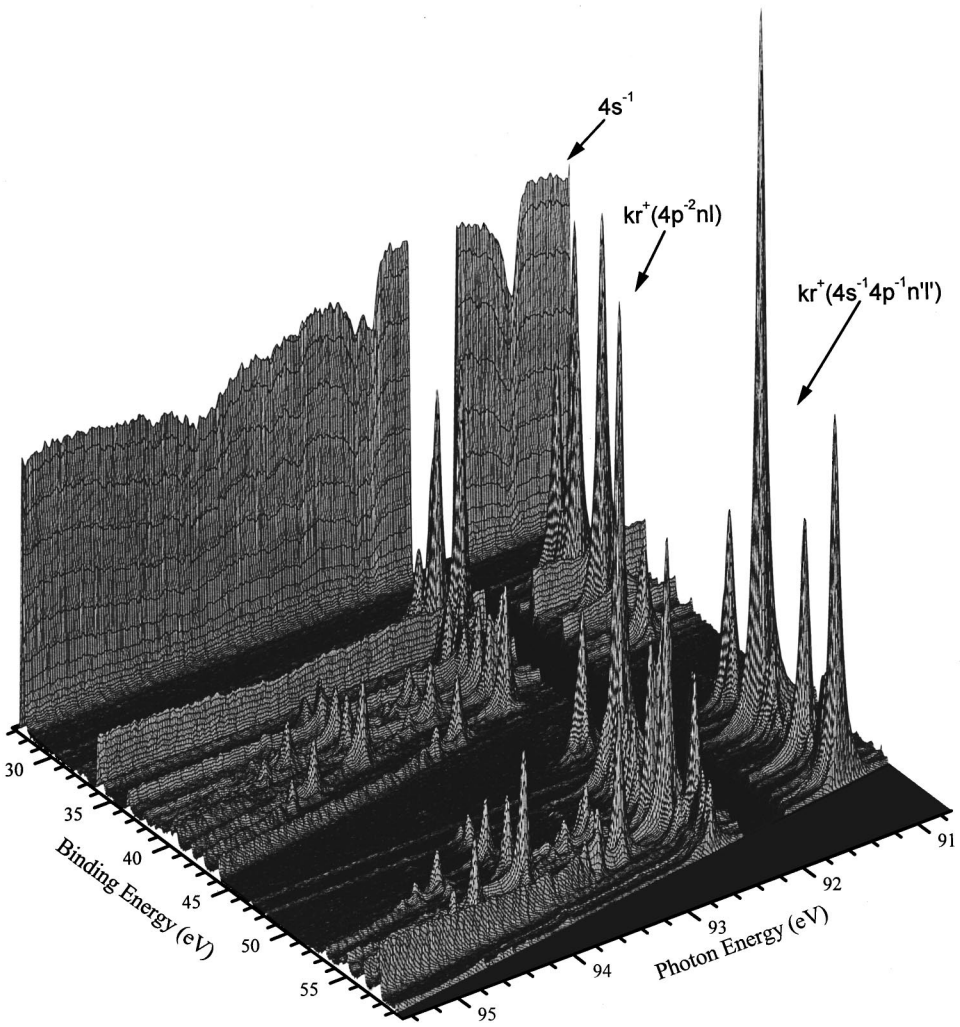

FIG. 1. Three-dimensional mapping of the resonant Auger landscape measured at 0° relative to the polarization plane.

mulated in a more general form by Arneberg, Müller, and Manne [16], who used second-quantization notation.

Recently, resonant Auger transitions and correlation satellite spectra of krypton have been the subject of both experimental [17–22] and theoretical [22–24] studies that have concentrated on the decay to the Kr^+ $4s^24p^{-2}mp$ states. In contrast, the Auger decay spectra of the Kr $3d^{-1}np \rightarrow 4s^{-1}4p^{-1}(^1P)mp$ $(n=5-9,\ m=5-11)$ transitions have received much less attention [25,26]. The recent measurements by Mursu *et al.* [26] were made at the magic angle (54.7°) and so could not provide angular distribution information.

In this paper we present extensive experimental results on photoexcitation and photoionization processes in Kr in the region of the $3d$ ionization thresholds using angle-resolved photoelectron imaging spectroscopy in combination with photons from an undulator beam line of the Advanced Light Source (ALS) at Lawrence Berkeley National Laboratory. This work will concentrate on the $3d^{-1}np \rightarrow 4s^{-1}4p^{-1}(^1P)mp$ $(n=5-9,\ m=5-11)$ Auger decay transitions. We present the angular distributions of the resonant Auger electrons resulting from the decay of $3d^{-1}_{3/2,5/2} \rightarrow np$ states. In addition, spectator and shake probabilities for the $3d^{-1}np \rightarrow 4s^{-1}4p^{-1}(^1P)mp$ $(n=5-9,\ m=5-11)$ resonant Auger transition have been obtained for almost all the final $4s^{-1}4p^{-1}(^1P)mp$ $(m=5-11)$ states.

II. EXPERIMENTAL DETAILS

In a photoionization process using the dipole approximation (which is valid in our experimental configuration), the differential cross section for electrons emitted at an angle θ with respect to the electric-field vector in a plane perpendicular to the incident radiation is given by [27]

$$\frac{d\sigma_{if}(h\nu)}{d\Omega}(\theta)=\frac{\sigma_{if}(h\nu)}{4\pi}\left\{1+\frac{\beta_{if}(h\nu)}{4}\times\{1+3P_1\cos[2(\theta-\lambda)]\}\right\}, \qquad (1)$$

where σ_{if} is the partial cross section, β_{if} is the angular distribution anisotropy parameter, P_1 is the degree of linear polarization of the monochromatic light, which we determined to be 99%, and λ is the tilt angle between the synchrotron plane and the electric field (0° in this case). The angular dependence of the differential cross section can be ascribed solely to the β parameter, except at $\theta=54.7°$ (the magic angle), where the angular dependence drops out completely and the differential cross section is simply proportional to the partial cross section σ_{if}.

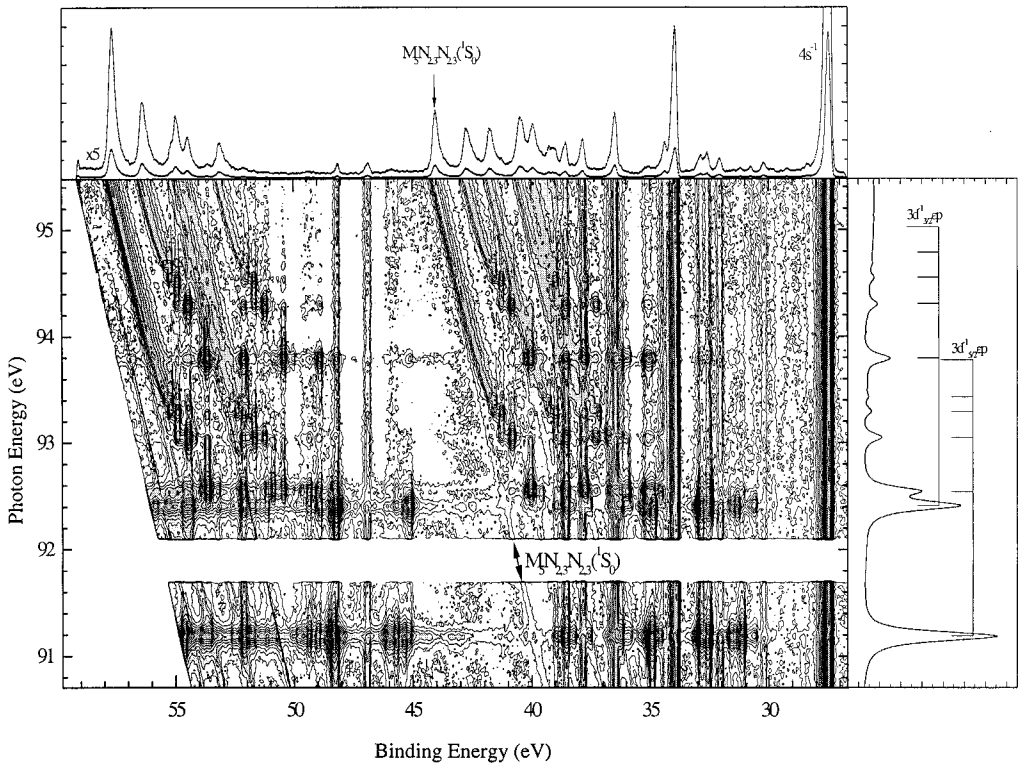

FIG. 2. Two-dimensional map showing Auger electron emissions of the Rydberg resonances measured at 0° relative to the polarization plane. The intensity of the electron signal is represented as different shades of gray, where darker regions indicate stronger intensities. The total electron yield spectrum and the photoelectron spectrum are shown on the right and on the top, respectively.

The experiment was performed in two-bunch operation mode at the ALS at Berkeley National Laboratory using the Atomic, Molecular and Optical Physics Undulator Beam line (9.0.1) equipped with a spherical grating monochromator. The measurements were carried out using two electron time-of-flight (TOF) analyzers mounted perpendicular to the axis of the incident photon beam. One analyzer was set at $\theta = 0°$ with respect to the electric-field vector of the incident radiation and the other at the magic angle. This configuration allowed us to record TOF spectra simultaneously at two different angles. Therefore, angular anisotropies could be measured and the β parameters could be extracted. Further aspects of the experimental apparatus are described in another work [28]. In the present experiment, krypton gas was introduced into the chamber interaction region through a needle up to a chamber pressure of about 3×10^{-5} Torr. In the interaction region we estimate a gas pressure that is about 8 times higher.

In this experiment, the photoelectron yield is collected and will be presented as a function of binding energy and photon energy in such a way as to show the various ionization processes of interest at a glance. This is achieved by accumulating photoelectron spectra simultaneously in each analyzer for 10 s at each photon energy. This energy was then incremented by 10 meV (typically $\frac{1}{4}$ of the photon resolution) followed by the collection of another pair of spectra. By repeating this procedure over the photon energy range of interest (90–96 eV), which took a total of 9000 s, we were able to produce comprehensive and detailed two-dimensional (2D) images of ionization processes at two emission angles. The photon energy step size was changed to 100 meV between the $3d_{5/2}^{-1}5p$ and $3d_{3/2}^{-1}5p$ resonances where no resonances are expected. Also, in order to improve the energy resolution for the collected electrons of interest, a 30-V retarding voltage was used to increase the electron flight time [28]. Once collected and displayed, more conventional one-dimensional spectra were extracted from the 2D data to allow more quantitative observations and comparisons to be made.

All TOF spectra require conversion from their initial time domain to kinetic energy. This was achieved by collecting TOF spectra of the Ne, which included the $2s$ and $2p$ photoelectron lines, at various photon energies. This produces a set of points (two for each photon energy) on the kinetic energy vs time-of-flight curve, which can then be used to convert between the two domains. The same data were also used to determine the transmission efficiency as a function of kinetic energy by a comparison with both partial cross section and β values available in the literature [29]. In addition, all spectra have been corrected for variations in the incident light intensity and a background level of scattered electrons has been removed, which is important when obtaining β values. The photon energy scale was calibrated using the Kr $(3d^{-1})np$ resonance energies of King *et al.* [30] and the binding-energy scale was calibrated by using the optical data of Minnhagen [31].

III. RESULTS AND DISCUSSION

A three-dimensional landscape of the resonant Auger emission is presented in Fig. 1, which was obtained at an angle of 0° relative to the photon polarization plane. The z

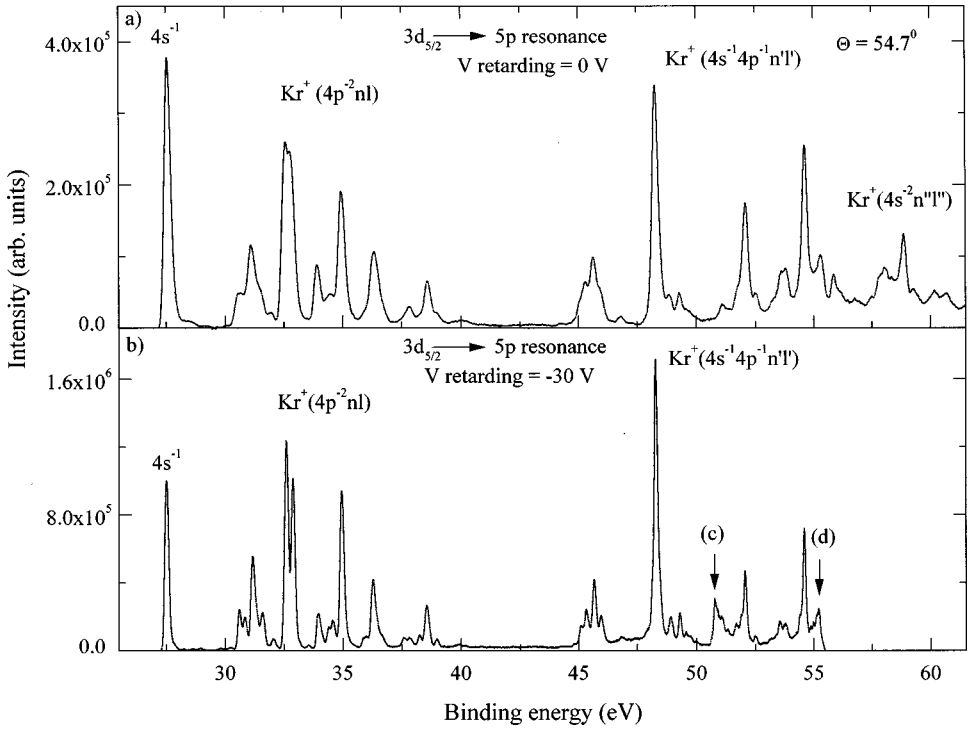

FIG. 3. Photoelectron spectrum of the $3d_{5/2}\rightarrow 5p$ resonance taken at 54.7° with respect to the electric-field vector of the incident radiation (a) collected with no retarding potential and (b) collected with a −30-V retarding potential. The two data sets were calibrated with two different transmission functions due to the two retarding voltages.

axis represents the intensity, the y axis the photon energy, and the x axis the binding energy. This figure gives a sense of the extent of the competition between participator (Kr^+ $4s^{-1}$) and spectator (Kr^+ $4s^2 4p^4 nl$ and $4s^1 4p^5 n'l'$) decay processes. The Kr^+ $4s^{-1}$ participator channel clearly shows asymmetric line profiles at the lower-lying resonances, while the spectator decay channels show up as peaks all over the ionization landscape.

To get a more detailed view of this information, the projection of the intensity onto the x-y plane is presented in Fig. 2 as a contour map with gray levels added to indicate higher intensities (increasing from light to dark). The total electron yield spectrum and the photoelectron spectrum are shown at the side and the top of this 2D map. This 2D contour map allows examination of all the data in a single figure from which features can be identified for more detailed analysis. It also has the advantage that it allows us to quickly observe certain types of experimental artifacts, such as peaks due to higher-order light or very slow electrons from an earlier photon pulse, to be identified and removed where possible from the 2D data. In this paper we will concentrate on the evolution Auger decay processes of the $3d\rightarrow np$ Rydberg series $n=5-11$ over a photon energy range of 6 eV. To produce 2D electron emission data sets, a photon energy range of 6 eV and a kinetic-energy window covering the majority of the ejected electrons of interest, corresponding to the Kr^+ $4s^2 4p^4 nl$ and $4s^1 4p^5 n'l'$ ionic states, was chosen. This allows a detailed investigation of the Kr $3d$ photoexcitation/ionization/relaxation processes in the resonance region below the threshold up to a few eV above the ionization limit.

The photon energy region covered in the 2D map can be broken down into three parts: (a) the low-lying $3d^{-1}np$ ($n=5-9$) resonances, (b) the merging of the high-lying

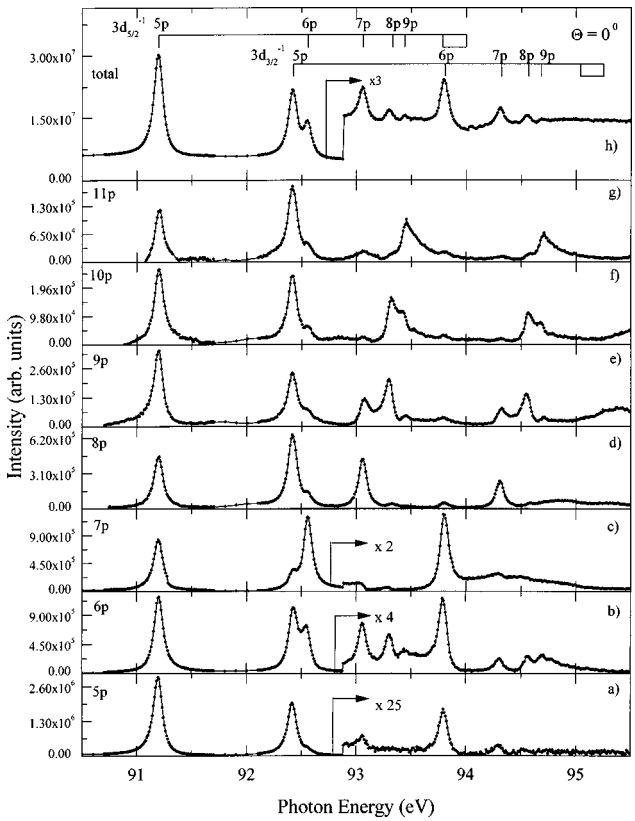

FIG. 4. (a)–(g) Constant ionic state spectra of the Kr^+ np ($n=5-11$) state extracted from the 2D display at 0° relative to the polarization plane. The total electron yield is shown in (h).

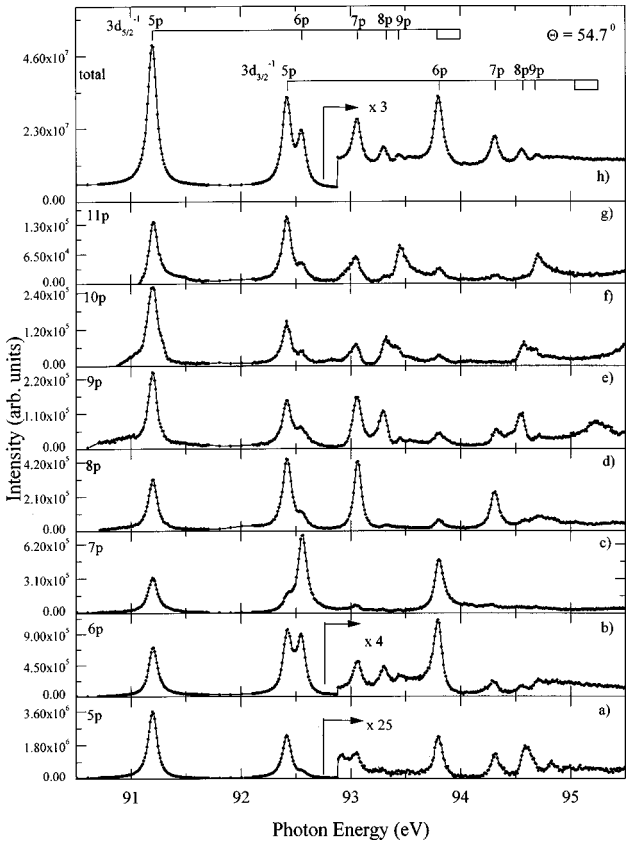

FIG. 5. (a)–(g) Constant ionic state spectra of the Kr^+ np ($n=5-11$) state extracted from the 2D display at 54.7° relative to the polarization plane. The total electron yield is shown in (h).

resonances and the ionization edges to which they converge, and (c) the $3d$ ionization that is followed by Auger decay, which results in spectral lines that exhibit shifting and broadening due to postcollision interaction (PCI) between the two outgoing electrons. In the case of (a), the low-lying resonances decay preferentially by Auger emission where the angular momentum of the Rydberg electron is unchanged but may undergo changes in its principal quantum number.

In the case of (b), the resonant states lying just below the $3d$ ionization threshold can be excited at the same photon energy at which ionization is also possible, due to the essentially constant resonance linewidth (83 meV) observed for these states, which is set by the core hole lifetime and not the Rydberg electron. When the photon energy is in the region of the ionization threshold, the shake-down lines becomes more important and merge smoothly into the high-kinetic-energy tail of the PCI-broadened normal Auger lines [22]. Details of how this evolution takes place is not clear from a theoretical point of view [32].

In the case of (c), the so-called normal Auger decay appears in the 2D map along diagonal lines, which represent the direction of constant kinetic energy. This decay involves the ejection of an inner-shell electron into the continuum followed by the decay of another electron to the inner-shell vacancy and the simultaneous ejection of a second electron, leaving a doubly ionized ion core [33]. The Auger lines, however, exhibit shifting and broadening due to the PCI since the slow photoelectron and the much faster Auger electrons can interact while still in the field of the nucleus since

TABLE I. Experimental spectator and shake probabilities [in percentage of the total intensities of all the $4s^{-1}4p^{-1}(^1P)mp$] resonances for the $3d^{-1}np \rightarrow 4s^{-1}4p^{-1}(^1P)mp$ ($n=5-9$, $m=5-11$) resonance Auger transitions. The statistical uncertainty of the last digits is given in parentheses. The shake-up of $m=n+1$ preferred is shown in boldface.

	Resonant state $3d^{-1}np$																					
	$n=5$				$n=6$				$n=7$				$n=8$				$n=9$					
	$3d_{5/2}^{-1}$		$3d_{3/2}^{-1}$		$3d_{5/2}^{-1}$		$3d_{3/2}^{-1}$		$3d_{5/2}^{-1}$		$3d_{3/2}^{-1}$		$3d_{5/2}^{-1}$		$3d_{3/2}^{-1}$		$3d_{5/2}^{-1}$		$3d_{3/2}^{-1}$			
Final ionic state	This work	Ref. [26] Expt./Calc.	This work	Ref. [26] Expt./Calc.	This work	Ref. [26] Expt./Calc.	This work	Ref. [26] Expt./Calc.	This work	Ref. [26] Expt./Calc.	This work	Ref. [26] Expt./Calc.	This work	Ref. [26] Expt./Calc.	This work	Ref. [26] Expt./Calc.	This work	Ref. [26] Expt.	This work	Ref. [26] Expt.		
$4s^{-1}4p^{-1}(^1P)5p$	64.3(4)	75/77	56.6(5)	18/8	8.2(3)	18/8	9.2(3)	7/8														
$4s^{-1}4p^{-1}(^1P)6p$	13.0(3)	20/22	21.2(5)	20/23	42.1(7)	29/35	28.7(6)	27/33	9.8(3)	10/10	9.2(3)	9/10	5.7(3)	18/4	5.6(2)	11/4	1.7(3)	9	1.1(3)	10		
$4s^{-1}4p^{-1}(^1P)7p$	5.9(3)	5/0	1.7(3)	5/0	41.1(6)	53/56	46.1(5)	66/57	2.2(4)	5/4	2.5(3)	0/4	0.4(4)	4/4	1.6(3)		1.3(3)	5	1.8(4)			
$4s^{-1}4p^{-1}(^1P)8p$	5.3(2)		11.0(3)		3.3(3)		5.1(2)		**37.1(8)**	73/73	**47.2(5)**	73/74	1.5(3)	6/2	4.1(2)	3/0		6	2.1(3)			
$4s^{-1}4p^{-1}(^1P)9p$	4.1(2)		3.3(2)		3.1(3)		5.2(3)		25.1(5)	12/10	38.3(7)	18/10	**40.7(5)**	43/57	**44.4(7)**	54/57	4.3(2)	11	1.5(4)	7		
$4s^{-1}4p^{-1}(^1P)10p$	5.3(4)		3.0(5)		1.0(4)		2.0(3)		16.0(6)				29.0(4)	30/31	41.7(6)	32/31	**67.8(6)**	38	60.2(5)	36		
$4s^{-1}4p^{-1}(^1P)11p$	2.1(8)		3.2(6)		1.2(5)		3.7(4)		9.8(4)		2.8(4)		22.7(4)		2.6(3)		24.9(5)	31	33.3(5)	40		

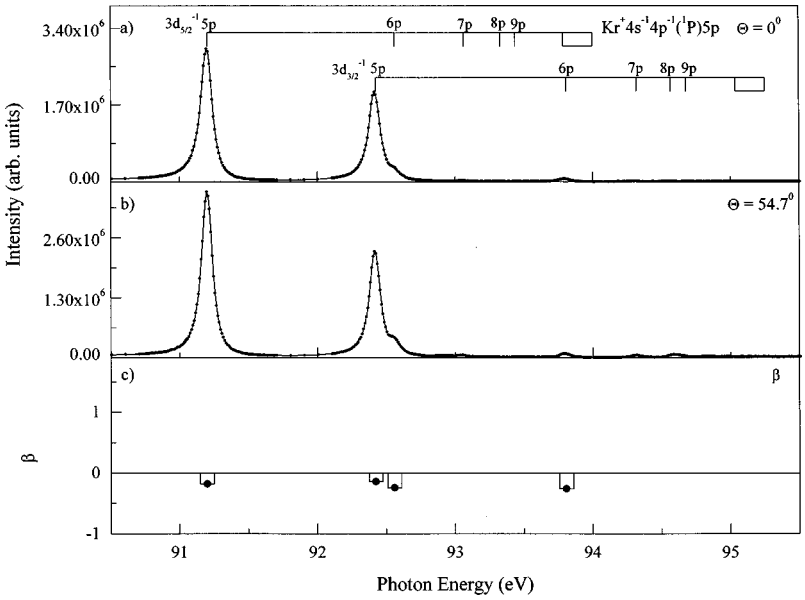

FIG. 6. Constant ionic state spectra of the Kr^+ $5p$ state extracted from the 2D display at two different angles, (a) 0° and (b) 54.7°, relative to the polarization plane. (c) Angular distribution parameter β for the $3d^{-1}np \rightarrow 4s^{-1}4p^{-1}(^1P)5p$ $(n=4-9)$ resonance Auger transitions.

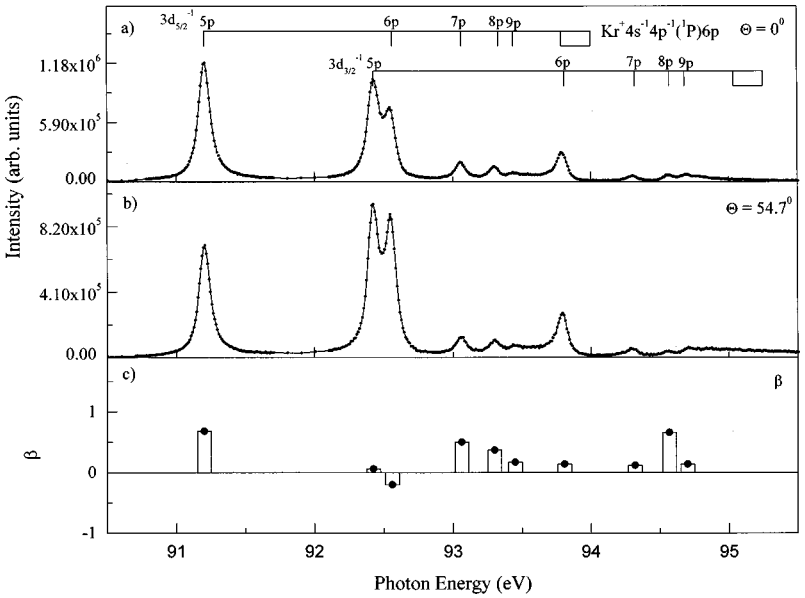

FIG. 7. Constant ionic state spectra of the Kr^+ $6p$ state extracted from the 2D display at two different angles, (a) 0° and (b) 54.7°, relative to the polarization plane. (c) Angular distribution parameter β for the $3d^{-1}np \rightarrow 4s^{-1}4p^{-1}(^1P)6p$ $(n=4-9)$ resonance Auger transitions.

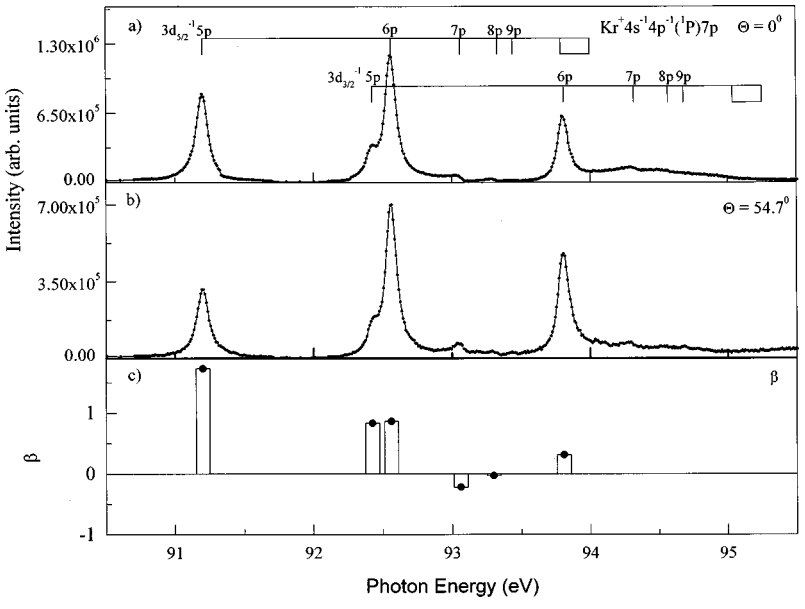

FIG. 8. Constant ionic state spectra of the Kr^+ $7p$ state extracted from the 2D display at two different angles, (a) 0° and (b) 54.7°, relative to the polarization plane. (c) Angular distribution parameter β for the $3d^{-1}np \rightarrow 4s^{-1}4p^{-1}(^1P)7p$ $(n=4-9)$ resonance Auger transitions.

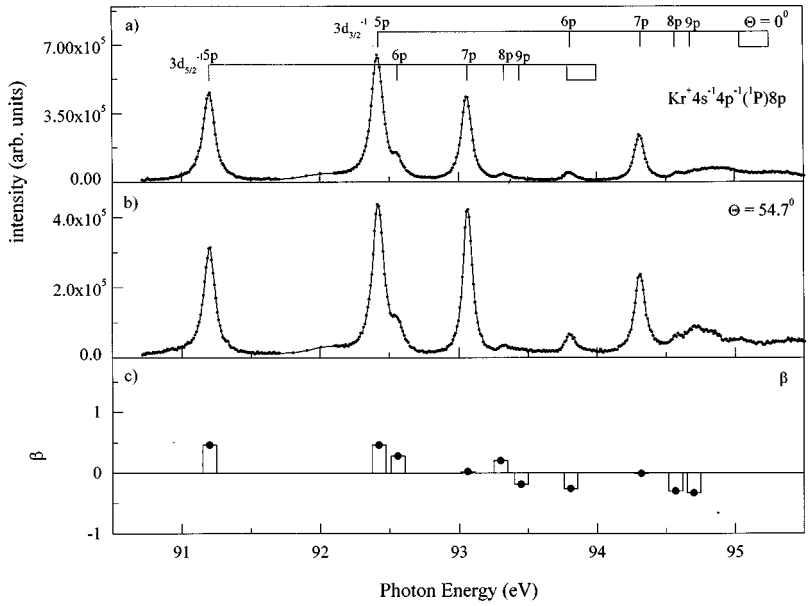

FIG. 9. Constant ionic state spectra of the Kr^+ $8p$ state extracted from the 2D display at two different angles, (a) 0° and (b) 54.7°, relative to the polarization plane. (c) Angular distribution parameter β for the $3d^{-1}np \rightarrow 4s^{-1}4p^{-1}(^1P)8p$ $(n=4-9)$ resonance Auger transitions.

the core hole lifetime is so short. The effect is most clearly seen in Fig. 2 for the $M_5N_{2,3}N_{2,3}(^1S_0)$ Auger line, where there is also a visible trace of the same line (produced by higher-order light) to the higher-binding-energy side (i.e., lower kinetic energy) throughout the photon energy range covered. Since here the photon energy is much higher, the photoelectron is consequently much farther away from the atom before the Auger electron is ejected and so PCI effects are no longer important.

In order to analyze the details and obtain quantitative information, we extracted photoelectron spectra from the 2D map. Figure 3(a) shows a photoelectron spectrum measured at an angle of 54.7° with respect to the electric-field vector of the photon beam. The photon energy of 91.2 eV corresponds to the Kr $3d_{5/2}5p$ resonance. This spectrum displays on resonance the population of the Kr $4s^{-1}$, $4p^{-2}nl$, $4s^{-1}4p^{-1}n'l'$, and $4s^{-2}n''l''$ ionic states. TOF analyzers have an energy resolution that is a function of the kinetic energy of the electrons, with the best resolution at lowest kinetic energies. Under the present conditions, the best resolution was 110 meV, decreasing to 147 meV at the highest kinetic energies of interest. The photon energy resolution was set to 40 meV at 90 eV. Clearly, one can see that the overall intensity of the lines resulting from transitions to the Kr^+ $4s^{-1}4p^{-1}n'l'$ states is similar to that of the transitions to the Kr^+ $4p^{-2}nl$ states (the ratio of the intensities of the two groups of lines was 1.2). Similar results have been seen in the case of the Xe $5s^{-1}5p^{-1}n'l'$ and Xe $5p^{-2}nl$ following the Xe $4d_{3/2} \rightarrow 6p$ decay [34]. In order to study the $4s^{-1}4p^{-1}n'l'$ ionic states with optimum resolution, we used a retarding voltage of -30 V on the TOF analyzers. It should be noted that in Fig. 3(b), the peak *c* arises from an experimental artifact and peak *d* is at the cutoff point of the spectrum caused by our choice of retarding voltage.

Figures 4 and 5 (0° and 54.7°, respectively) show constant ionic state spectra of Kr^+ np $(n=5-11)$ in panels (a)–(g), which have been extracted from the 2D data sets at the two different angles. Panel (b) in Figs. 4 and 5 shows the total

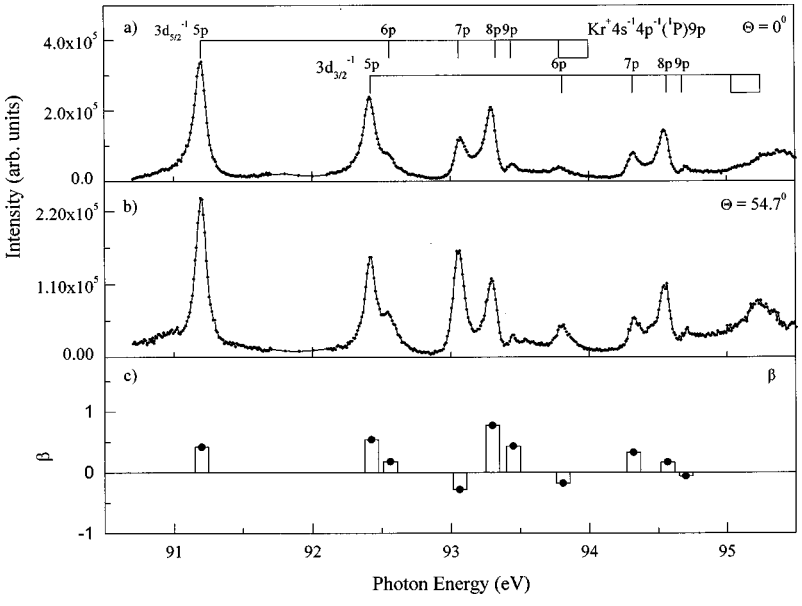

FIG. 10. Constant ionic state spectra of the Kr^+ $9p$ state extracted from the 2D display at two different angles, (a) 0° and (b) 54.7°, relative to the polarization plane. (c) Angular distribution parameter β for the $3d^{-1}np \rightarrow 4s^{-1}4p^{-1}(^1P)9p$ $(n=4-9)$ resonance Auger transitions.

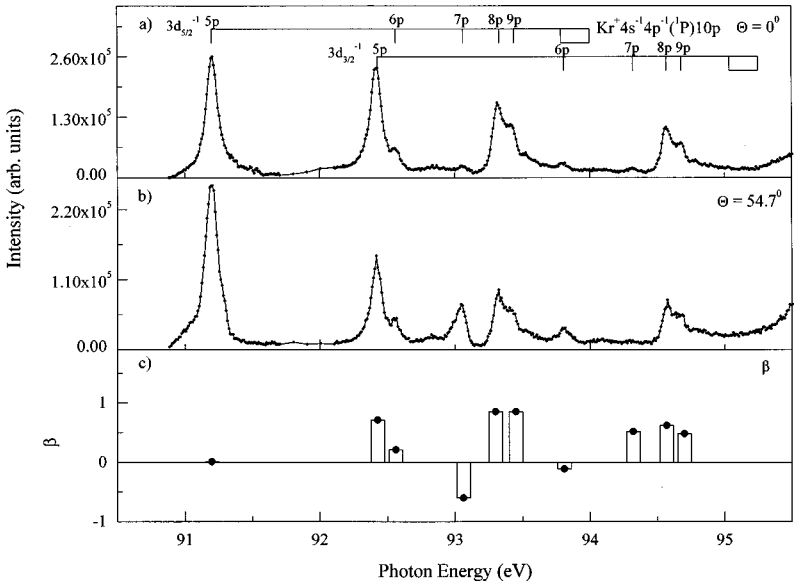

FIG. 11. Constant ionic state spectra of the Kr^+ $10p$ state extracted from the 2D display at two different angles, (a) 0° and (b) 54.7°, relative to the polarization plane. (c) Angular distribution parameter β for the $3d^{-1}np \rightarrow 4s^{-1}4p^{-1}(^1P)10p$ $(n=4-9)$ resonance Auger transitions.

electron yield. An asymmetry can be observed at the low-photon-energy side of the $3d_{5/2}^{-1}5p$ resonance in panels (e)–(g) for both Figs. 4 and 5, respectively. This is due to lines arising from higher-order photons, which happen to coincide with the edge of the resonance. In Fig. 5(a) there are over-enhanced intensities for the resonances in the (92.8–96)-eV range. This arises from very slow electrons, also resonantly enhanced, from the previous photon pulse crossing this final ionic state.

Assignments and experimental shake-up probabilities for each $4s^{-1}4p^{-1}(^1P)np$ final state are given in Table I. The experimental shake-up probabilities were obtained as a percentage of the total intensity of all the $4s^{-1}4p^{-1}(^1P)np$ final states at each resonance. The statistical uncertainty in the last digits is given in parentheses. The assignments have been made by comparison with the quantum defects obtained from previously measured Kr^+ $4s^24p^4(^SL_J)ns$, np, and nd states [21]. The best agreement is with the Kr^+ $(^SL_J)np$ Rydberg states. It is very clear from Table I that the spectator-core coupling is very strong in the decay of $3d^{-1}5p \rightarrow 4s^{-1}4p^{-1}(^1P)5p$ and $3d^{-1}6p \rightarrow 4s^{-1}4p^{-1}(^1P)6p$ excitations. In the region where the resonance lines are well separated $(n=7-9)$, the probabilities of the spectator transition become very small (less than 9%) and shake-up processes [Kr^+ np to Kr^+ $(n+1)p$] become very important. A comparison of these results with measurements and theoretical calculations made by Mursu *et al.* [26] showed a similar behavior as indicated in Table I. However, Mursu *et al.* did not include some of $4s^{-1}4p^{-1}(^1P)np$ states as shown in Table I. Although our esults and those of Mursu *et al.* are in reasonable agreement, it is possible that the discrepancy is due to the fact that they did not include all the states. In our case, we include states up to $n=11$ in the case of the $3d^{-1}5p \rightarrow 4s^{-1}4p^{-1}(^1P)np$ excitation, while they include only the first three final states $(n=7)$. Similar behavior has been found in the decay of the $3d^{-1}5p \rightarrow 4p^{-2}5p$ and the $3d^{-1}6p \rightarrow 4p^{-2}6p$ excitations in Kr by Jauhiainen *et al.* [21]. The probability for the $3d_{5/2}^{-1}5p \rightarrow 4s^{-1}4p^{-1}(^1P)6p$ excitation was found to be 13%. Significantly higher

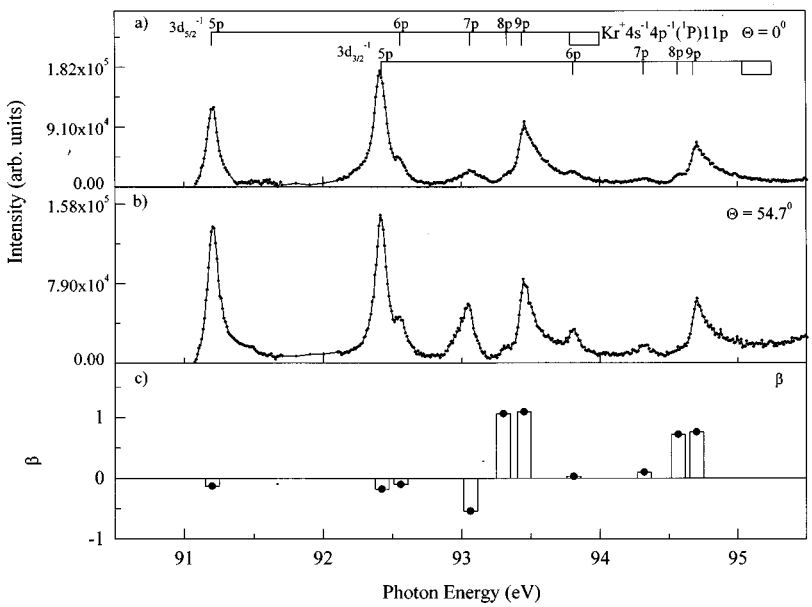

FIG. 12. Constant ionic state spectra of the Kr^+ $11p$ state extracted from the 2D display at two different angles, (a) 0° and (b) 54.7°, relative to the polarization plane. (c) Angular distribution parameter β for the $3d^{-1}np \rightarrow 4s^{-1}4p^{-1}(^1P)11p$ $(n=4-9)$ resonance Auger transitions.

TABLE II. Experimental angular distribution anisotropy parameters β for the $3d^{-1}np \rightarrow 4s^{-1}4p^{-1}mp$ ($n=5-9$, $m=5-11$) resonance Auger transitions. For each β value, the uncertainty is given in parentheses. The angular distributors close to being isotropic are shown in boldface.

	Resonant state $3d^{-1}np$									
	$n=5$		$n=6$		$n=7$		$n=8$		$n=9$	
Final ionic state	$3d_{5/2}^{-1}$	$3d_{3/2}^{-1}$	$3d_{5/2}^{-1}$	$3d_{3/2}^{-1}$	$3d_{5/2}^{-1}$	$3d_{3/2}^{-1}$	$3d_{5/2}^{-1}$	$3d_{3/2}^{-1}$	$3d_{5/2}^{-1}$	$3d_{3/2}^{-1}$
$4s^{-1}4p^{-1}(^1P)5p$	**−0.18(6)**	**−0.14(5)**	−0.24(8)	−0.26(9)						
$4s^{-1}4p^{-1}(^1P)6p$	0.68(16)	0.06(2)	**−0.20(5)**	**0.14(4)**	0.50(12)	0.12(3)	0.37(9)	0.66(15)	0.17(4)	0.14(3)
$4s^{-1}4p^{-1}(^1P)7p$	1.73(17)	0.83(8)	0.86(9)	0.31(3)	**−0.22(2)**		−0.03(3)			
$4s^{-1}4p^{-1}(^1P)8p$	0.46(11)	0.46(11)	0.28(7)	−0.26(6)	0.02(5)	−0.01(3)	**0.20(5)**	**0.30(8)**	−0.19(5)	−0.33(8)
$4s^{-1}4p^{-1}(^1P)9p$	0.42(10)	0.54(13)	0.18(5)	−0.18(5)	−0.28(7)	0.33(8)	0.77(19)	0.17(4)	**0.43(11)**	**−0.06(2)**
$4s^{-1}4p^{-1}(^1P)10p$	0.01(2)	0.71(17)	0.21(5)	−0.11(3)	−0.60(15)	0.52(13)	0.9(2)	0.62(15)	0.9(2)	0.48(12)
$4s^{-1}4p^{-1}(^1P)11p$	−0.13(3)	−0.18(5)	−0.10(3)	0.03(2)	−0.54(13)	0.10(3)	1.1(3)	0.72(18)	1.1(3)	0.76(19)

shake-up probability (21%) can be seen in the case of $3d_{3/2}^{-1}5p \rightarrow 4s^{-1}4p^{-1}(^1P)6p$ excitation, which is also found for the decay to the $4p^{-2}np$ case [21]. This similarity is extended to a comparison with the Xe $4d^{-1}6p$ resonances [35], where we notice that the shake probabilities behaved exactly the same way.

Åberg [32], in his theoretical work, has explained the shake probability $P_{nn'}=|\langle nlj|n'lj\rangle|^2$, where the orbital $|n'lj\rangle$ is evaluated in the field of the singly charged ion with the hole in the subshell $n_i l_i j_i$, whereas $|nlj\rangle$ must be evaluated in the field of the final doubly charged ion. He found that the probability of the spectator electron $P_{nn'}$ changes as a function of n'. The maximum values of $P_{nn'}$ become smaller and the shake-up probability becomes more important as n' increases. Comparing our experimental results with his theoretical prediction gives good agreement.

Figures 6–12 show the comparison of the $3d^{-1}np \rightarrow 4s^{-1}4p^{-1}(^1P)mp$ ($n=5-9$, $m=5-11$) transitions measured at both angles. Table II shows the experimental β values extracted from the $3d^{-1}np \rightarrow 4s^{-1}4p^{-1}(^1P)mp$ ($n=4-9$, $m=5,11$) resonance Auger transitions. For each β value, the uncertainty in the last digit is given in parentheses. These have been estimated by comparing β values for the $3d_{5/2}^{-1}5p \rightarrow 4s^{-1}4p^{-1}(^1P)5p$ transition from two independent data sets (0- and 30-V retarding potentials). From the table we can note that close to isotropic angular distributions are observed for most of the $3d^{-1}np \rightarrow 4s^{-1}4p^{-1}(^1P)mp$ ($n=m$) strict spectator decays, while for decays involving shake-up ($m>n$) or shake-down ($m<n$) larger anisotropies are seen. According to the prediction of the general strict spectator model, which was introduced by Hergenhahn, Kabachnik, and Lohmann [5], these β values have to be zero, which agrees qualitatively with our experimental observations. When the $3d$ electrons are excited to the $7p$ or higher Rydberg orbitals (Figs. 8–12), the strength of the spectator-core coupling diminishes, the shake-up transition becomes dominant, and a fluctuation of β values is observed. This angular information now awaits theoretical treatment.

IV. CONCLUSION

We have studied the resonant Auger decay following photoionization of the $3d$ inner-shell orbital in krypton. The use of the angle-resolved two-dimensional acquisition technique has enabled us to observe various processes over a large kinetic-energy and photon energy range. Spectator and shake probabilities for the $3d^{-1}np \rightarrow 4s^{-1}4p^{-1}(^1P)mp$ ($n=5-9$, $m=5,11$) resonance Auger transition have been studied and compared with previous non-angular-resolved measurements and theoretical calculation by Mursu *et al.* [26]. Our results show that the spectator-core coupling is strong at lower-n excitation but lessens when higher-n resonances are excited and the shake-up transition becomes dominant. We also show at higher Rydberg n the importance of the one-step shake-up processes. The comparison of our results with previous measurements and theoretical calculation for the $3d^{-1}np \rightarrow 4s^{-1}4p^{-1}(^1P)mp$ [26] and $3d^{-1}np \rightarrow 4p^4mp$ resonance Auger transitions [21] and theoretical prediction [32] shows good agreement.

Angular distributions of the Auger electrons resulting from the decay of the resonantly excited $3d^{-1}np$ states in krypton have been derived. Small-β values have been observed when lower resonances are excited where the strict spectator model is assumed to be most valid, but the values of β fluctuate at higher resonances. We hope that this paper, which is an angular distributions study on the $3d^{-1}np \rightarrow 4s^{-1}4p^{-1}(^1P)mp$ resonance Auger transitions, will stimulate further experimental and theoretical work on these inner-shell processes.

ACKNOWLEDGMENT

This work was supported by the U.S. Department of Energy, Office of Basic Energy Science, Division of Chemical Sciences under Contract No. DE-FG02-95ER14299.

[1] W. Eberhardt, G. Kalkoffen, and C. Kunz, Phys. Rev. Lett. **41**, 156 (1978).
[2] H. Aksela, S. Aksela, J. Tulkki, T. Åberg, G. M. Bancroft, and K. H. Tan, Phys. Rev. A **39**, 3401 (1989).
[3] S. B. Whitfield, C. D. Caldwell, D. X. Huang, and M. O. Krause, J. Phys. B **25**, 4755 (1992).
[4] T. A. Carlson, D. R. Mullins, C. E. Beall, B. W. Yates, J. W. Taylor, D. W. Lindle, and F. Grimm, Phys. Rev. A **39**, 1170 (1989).
[5] U. Hergenhahn, N. M. Kabachnik, and B. Lohmann, J. Phys. B **24**, 4759 (1991).
[6] H. Aksela, O.-P. Sairanen, S. Aksela, A. Kivimäki, A. Naves de Brito, E. Nmmiste, J. Tulkki, A. Ausmees, S. J. Osborne, and S. Svensson, Phys. Rev. A **51**, 1291 (1995).
[7] J. Mursu, H. Aksela, O.-P. Sairanen, A. Kivimäki, E. Nõmmiste, A. Ausmees, S. Svensson, and S. Aksela, J. Phys. B **29**, 4387 (1996).
[8] U. Becker, T. Perescher, E. Schmit, B. Sonntag, and H.-E. Wetzel, Phys. Rev. A **33**, 3891 (1986).
[9] U. Becker, D. Szostak, M. Kupsch, H.-G. Kerkhoff, B. Langer, and R. Wehlitz, J. Phys. B **22**, 749 (1989).
[10] U. Becker and R. Wehlitz, J. Electron Spectrosc. Relat. Phenom. **67**, 341 (1993).
[11] B. Langer, N. Berrah, A. Farhat, O. Hemmers, and J. D. Bozek, Phys. Rev. A **53**, R1946 (1996).
[12] A. Frahat, M. Humphery, B. Langer, N. Berrah, J. D. Bozek, and D. Cubaynes, Phys. Rev. A **56**, 501 (1997).
[13] T. Hayaishi, Y. Morioka, Y. Kageyama, M. Watanabe, I. H. Suzuki, A. Mikuni, G. Isoyama, S. Asaoka, and N. Nakamura, J. Phys. B **17**, 3511 (1984).
[14] T. Åberg, Ann. Acad. Sci. Fenn., Ser. AI: Math. **5**, 308 (1969).
[15] R. L. Martin and D. A. Shirley, Phys. Rev. A **13**, 1475 (1976).
[16] R. Ameberg, J. Müller, and R. Manne, Chem. Phys. **64**, 249 (1982).
[17] S. Svenssen, B. Eriksson, N. Mårtensson, G. Wendin, and U. Gelius, J. Electron Spectrosc. Relat. Phenom. **47**, 327 (1988).
[18] B. Kämmerling, B. Krässig, O. Schwarzkopf, J. P. Ribeiro, and V. Schmidt, J. Phys. B **25**, L5 (1992).
[19] H. Aksela, J. Jauhianien, E. Kukk, E. Nmmiste, S. Aksela, and J. Tulkki, Phys. Rev. A **53**, 290 (1996).
[20] A. Kikas, S. J. Osborne, A. Ausmees, S. Svensson, O.-P. Sairanen, and S. Aksela, J. Electron Spectrosc. Relat. Phenom. **77**, 241 (1996).
[21] J. Jauhianien, H. Aksela, O.-P. Sairanen, E. Nmmiste, and S. Aksela, J. Phys. B **29**, 3385 (1996).
[22] H. Aksela, M. Kivilompolo, E. Nmmiste, and S. Aksela, Phys. Rev. Lett. **25**, 4970 (1997).
[23] H. Aksela, S. Aksela, A. Mäntykenttä, J. Tulkki, E. Shigmasa, A. Yagishita, and Y. Furusawa, Phys. Scr. **T41**, 113 (1992).
[24] G. B. Armen, J. Phys. B **29**, 677 (1996).
[25] H. Aksela, S. Aksela, H. Pulkkinen, G. M. Bancroft, and K. H. Tan, Phys. Rev. A **33**, 3876 (1986).
[26] J. Mursu, J. Jauhiainen, H. Aksela, and S. Aksela, J. Phys. B **31**, 1973 (1998).
[27] H. Derenbach and V. Schmidt, J. Phys. B **17**, 83 (1984).
[28] B. Langer, A. Farhat, B. Nessar, N. Berrah, O. Hemmers, and J. D. Bozek, in *Proceedings of the Workshop on Atomic Physics with Hard X-Rays from High Brilliance Synchrotron Light Sources* (Argonne National Laboratory, Argonne, IL, 1996), 245.
[29] F. Wuilleumier and M. O. Krause, J. Electron Spectrosc. Relat. Phenom. **15**, 15 (1979).
[30] G. C. King, M. Tronc, F. H. Read, and R. C. Bradford, J. Phys. B **10**, 2479 (1977).
[31] L. Minnhagen, Ark. Fys. **25**, 203 (1963).
[32] T. Åberg, Phys. Scr. **T41**, 71 (1992).
[33] J. Berkowitz, *Photoabsorption, Photoionization, and Photoelectron Spectroscopy* (Academic, New York, 1979).
[34] N. Berrah, B, Langer, and A. Farhat, in *Proceedings of the Raman Emission by X-Rays (REX-1) Workshop*, edited by D. L. Ederer and J. H. McGuire (World Scientific, Singapore, 1996), p. 156.
[35] H. Aksela, S. Aksela, O.-P. Sairanen, A. Kivimäki, A. Naves de Brito, E. Nmmiste, J. Tulkki, S. Svensson, A. Ausmees, and S. J. Osborne, Phys. Rev. A **49**, R4269 (1994).